Characterization of nanostructure in low dose Fe-implanted p-type 6H-SiC using atom probe tomography

Lindor Diallo, Luc Lechevallier, Abdeslem Fnidiki, Jean Juraszek, M. Viret, A. Declemy

Characterization of nanostructure in low dose Fe-implanted p-type 6H-SiC Using Atom Probe Tomography

L. Diallo[1], L. Lechevallier[1, 2], A. Fnidiki[1], J. Juraszek[1], M. Viret[3], A. Declémy[4]

1. Normandie Univ., INSA Rouen, UNIROUEN, CNRS, GPM, 76800 Rouen, France
2. Département de GEII, Université de Cergy-Pontoise, rue d'Eragny, Neuville sur Oise, 95031 Cergy-Pontoise, France
3. Service de Physique de l'Etat Condensé (DSM/IRAMIS/SPEC), UMR 3680 CNRS, Bât. 772, Orme des Merisiers, CEA Saclay, 91191 Gif sur Yvette, France
4. Institut PPRIME, UPR 3346 CNRS, Université de Poitiers, ENSMA, SP2MI, téléport 2, 11 Bvd M. et P. Curie, 86962 Futuroscope, Chasseneuil, France

Abstract

P-doped 6H-SiC substrates were implanted with Fe ions. During implantation the samples were maintained at 550°C with energies ranging from 30 to 160 keV in order to produce a diluted magnetic semiconductor (DMS) with a 2 % Fe homogeneous concentration to a depth of about 100 nm thickness. The effects of rapid thermal annealing on the microstructure were examined by atom probe tomography (APT). The study shows evidence of the formation of Fe rich nanoclusters after annealing which contain core magnetic phases that contribute to the magnetic properties.

Keywords: Spin electronics, diluted magnetic semiconductor, atom probe tomography, nanoclusters

1. Introduction

Doping a semiconductor with a 3d magnetic element (Cr, Mn, Fe, Co) confers ferromagnetic (FM) properties, while keeping the semiconductor nature of the material. The discovery of DMSs with relatively high Curie temperatures (T_C), such as (In, Mn) As [1], and especially (Ga, Mn) As [2], has initiated a major international research effort over the last two decades, in order to understand the origin and the mechanism of the magnetic properties of these types of materials. Many advances have been made in the growth and annealing of these samples to minimize the presence of secondary phases or compensate defects that are detrimental to the desired properties. The possibility to achieve the T_C values higher than 300 K was forecasted for certain wide-gap DMSs with rather a high concentration of free holes [3]. This prognosis gave impetus to a great number of experiments aimed at the discovery of DMS materials with high T_C. Many authors reported that they observed ferromagnetism in the corresponding objects above room temperature. However, most of these observations later turned out to be the consequence of the presence of precipitates in the studied specimens or the inclusion of other phases of transition metal (TM) compounds in solid solutions to which the DMS specimens belong [4]. This circumstance stimulated the appearance of theoretical works, showing that the ferromagnetic (FM) ordering in such specimens can be partly explained by the exchange interaction between charge carriers and doping magnetic ions [5]. Still, despite this intense research in the DMSs field, no T_C higher than room temperature has ever been obtained. Moreover, the nature and origin of ferromagnetism in III-V compounds remain controversial [6]. Silicon Carbide (SiC) is a wide bandgap semiconductor that has been considered a possible candidate for spin electronics applications. SiC has a long history in materials research and device development and has already been commercialized for high-frequency and high power applications. A FM response has been experimentally observed in Ni, Mn and Fe doped 6H-SiC with the value of the T_C varying from significantly below to close to room temperature. The authors assigned the magnetic signal to the true DMS behavior [7-8]. According to Dupeyrat et al. [9] and Diallo et al. [10], the formation of Fe_3Si nanoscale particles is mainly responsible for the magnetic properties observed in 6H-SiC system implanted with a 6 at.% Fe ions concentration and annealed at a high temperature (> 900 °C). This is not the case according to ref 11 where authors demonstrate that the presence of Fe_3Si is not the origin

Corresponding authors: lindor.diallo@etu.uni-rouen.fr

of FM ordering in Fe-doped SiC. It also indicated that traces of Fe-doping in SiC induce a high temperature FM arrangement. Typical FM order was established for low Mn-doping concentrations (10^{-4} molar fraction) at around 250 K in 6H-SiC [12]. These authors found that defects-related effects other than the Mn content play the most important role in the magnetic ordering. Ferromagnetism was experimentally evidenced in 6H-SiC after neutron irradiation by Liu et al. [13]. Ab initio calculations using different computational techniques were used to theoretically study magnetic properties of SiC-based DMSs. Contradictions were also found in these results. Fe was found magnetic or nonmagnetic according to the structural configurations, while Cr and Mn were found to be magnetic at the substitutional Si site [14-16]. Recently Los et al. [16] reported that Fe in SiC matrix can exist in both magnetic and nonmagnetic states depending on the transition metal atom environment in the host matrix. For different impurity species, these authors found that the transition from the nonmagnetic to magnetic configuration and the corresponding changes of the atomic moments may take place either gradually, when the volume of the unit cell changes, or when the energy gap between the two states is overcome.

In recent communications [10, 17-18] it was shown that Fe atoms in the substitutional Si site lead to FM behavior in 6H-SiC. Here, we report about the characterization of the nanostructure in 2 at.% Fe implanted 6H-SiC by APT. This technique revealed a random distribution of Fe atoms in the SiC matrix in the as-implanted sample and the existence of Fe-rich nanoparticles in the annealed samples.

.

2. Material and Methods

Commercial (CREE) near (0001)-oriented n-type 6H-SiC substrates with a 200 nm thick uppermost p-type epitaxial layer (nA - nD ~10^{+20} Al/cm^3) were co-implanted with 30 to 160 keV $^{56}Fe^+$ ions. The dose reaches 10^{+16}/cm^2 leading to a Fe concentration of about 2 at.% at depth between 20 nm and 100 nm from the sample surface, checked by Rutherford Backscattering Spectrometry (RBS) at the CSNSM-Orsay [19,20]. The samples were held at 550 °C during implantation in order to avoid amorphisation [21]. After the implantation, the samples were subjected to a rapid thermal annealing at different temperatures (900 and 1300°C) for 4 min. The principle of the APT technique is based on field evaporation of surface atoms from a sample prepared in the form of a sharp needle (radius < 50 nm). The chemical identification of the sample atoms is based on the time-of-flight mass spectrometry technique. The evaporated atoms are collected on a position-sensitive detector that provides both time of flight and position of the incoming ions. This combined information allows deducing the chemical nature of the evaporated ions and the initial position at the specimen surface (sharp tips) [22]. A 3D reconstruction of the analyzed volume is generated, giving access to the spatial distribution of atoms at the atomic scale. Local chemical composition of any arbitrary sub volumes can be obtained with a sub-nanometric resolution. In particular, concentration profiles with a depth resolution better than half an atomic plane can be generated in metals [23]. APT specimens were prepared through the lift-off method and standard milling [24] using a dual beam SEM/FIB Zeiss Nvision 40. In order to reduce Ga implantation and avoid damages in the region of interest, the Fe-implanted SiC samples were capped with 500 nm of Pt and a final polishing was performed at low acceleration voltage (2 kV). The samples were analyzed by a Laser Flexible Tomographic Atom Probe (LAWATAP) at 80 K in an ultrahigh vacuum chamber under a pressure of 10^{-8} Pa. The used femtosecond laser pulse system was an amplified ytterbium-doped laser (AMPLITUDE SYSTEM s-pulse HR) with a pulse period of 350 fs and a 100 kHz repetition rate. The wavelength was fixed at 342 nm.

3. RESULTS and DISCUSSION

3.1. Structural and chemical composition

A typical mass spectrum of 6H-SiC implanted with a 2 at.% Fe concentration and annealed at 1300 °C is shown in Fig. 1. C atoms evaporate in the form of single or molecular ions in these conditions. The peak at 28 amu (atomic mass unit) is assigned to the $^{56}Fe^{2+}$ isotope. Si^{2+} ions are detected predominantly in the second charge state at 14, 14.5, and 15 amu. Al^{3+} ions were also detected which correspond to the p-doping species in these samples.

Corresponding authors: lindor.diallo@etu.uni-rouen.fr

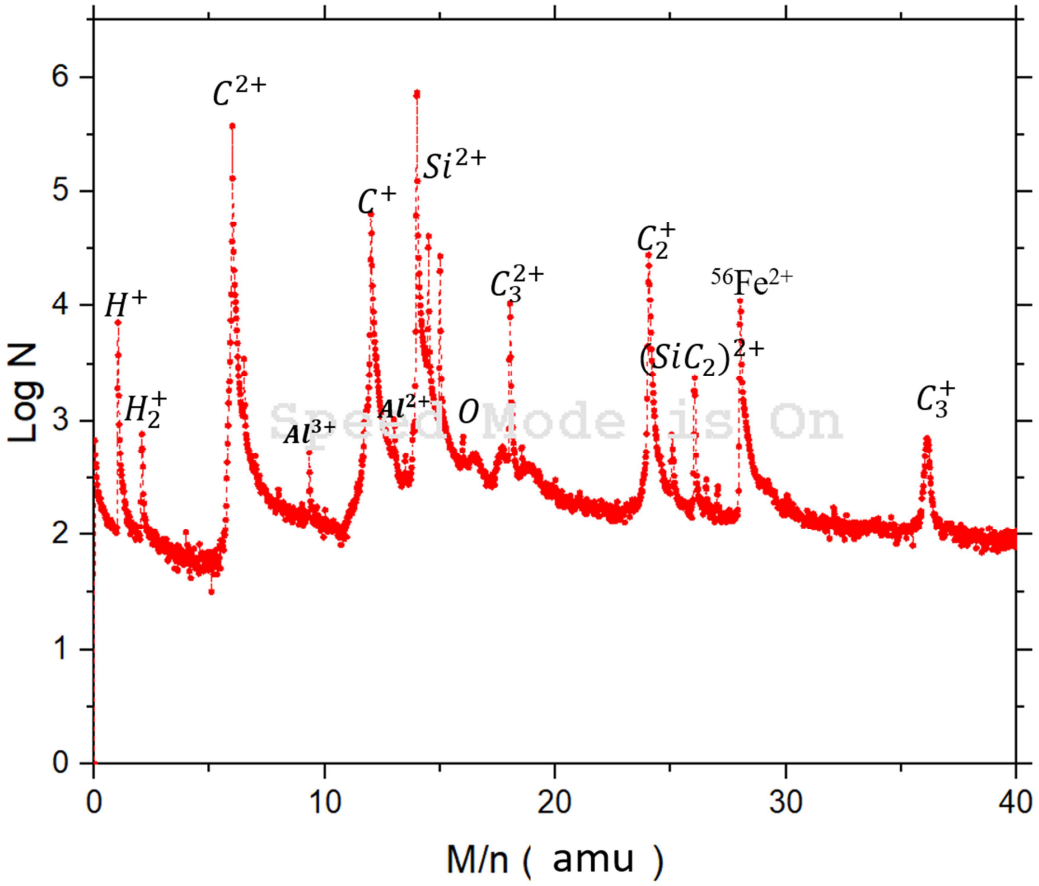

Fig. 1. Mass spectrum of the 1300°C annealed Fe-implanted 6H-SiC sample

Fig. 2 shows a 3D reconstruction of the same sample. The volume of reconstruction is 70 x 70 x 73 nm^3. The APT pattern evidences the presence of nano-sized Fe-rich nanoparticles, represented in this figure with different colors. The average concentrations of Si, C and Fe atoms over the entire analyzed volume are 50.1 ± 0.1%, 46.3 ± 0.1 and 1.9 ± 0.1%, respectively. The sum of these three elements being 98.3 at.%, the remainder (1.7 %) consists of Al and O atoms, corresponding to the initial electrical doping of SiC and the oxidation of the material, respectively. We also can observe that the Si and C concentrations are not exactly the same. This is due to the presence of molecular species such as C_2 and C_3 and to the difficulty to separate, for example, the two C^+ and C_2^{2+} species obtained for the same M/n ratio (12 amu). Thus, it results that the uncertainty on the C concentration is perhaps weakly higher than ± 0.1 % but remains of the same order.

Corresponding authors: lindor.diallo@etu.uni-rouen.fr

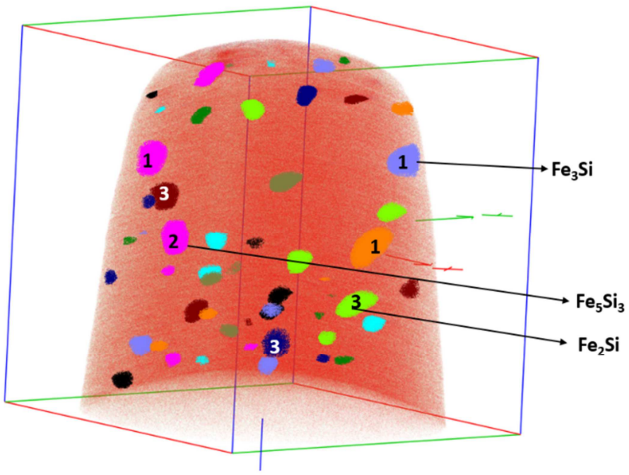

Fig. 2. 3D reconstruction of the 1300°C annealed Fe-implanted 6H-SiC sample showing the spatial distribution of Fe atoms in a 70 x 70 x 73 nm^3 volume in a red color matrix. Nanoparticles are represented with different colors and their associated phases (Fe_3Si, Fe_5Si_3, Fe_2Si) are indexed with the numbers (1, 2, 3), respectively

3.2 Nanoparticle compositions

The identification of clusters makes it possible to label each Si, Fe or C atom belonging to the different nanoparticles and thus to measure the average compositions of the Fe-rich nanoparticles. The average Fe concentration varies versus the average diameter of nanoparticles. It is 39, 51 and 64 at.% for nanoparticles having an average diameter of 6, 7 and 10 nm, respectively. For each identified nanoparticle, an associated mass spectrum is obtained and a radial profile is plotted. It can be noted that the largest nanoparticles contain several tens of thousands of Fe, Si and C atoms and the smallest ones contain a few tens of atoms, only. The core phases are identified by reporting the concentrations obtained in the central part of the nanoparticles in a sphere having a 1 nm diameter. The Fe atoms concentration varies greatly from one nanoparticle to another, indicating the presence of (FeSi) rich phases containing small C amounts. The values of the Si, C and Fe concentrations depend, as observed above, on the different atomic or molecular evaporated species as well as on the reconstruction artifacts of the APT which introduce position errors of atoms. Indeed, the difference of evaporation fields between the atoms located in the nanoparticles and in the matrix leads to local magnification effects in the reconstruction process, which decreases the spatial resolution. In our case, the nanoparticles are mainly composed of (Fe-Si) phases which are evaporated under a low evaporation field, close to the Fe evaporation field (i.e. E_{Fe} ~ 33 $V.nm^{-1}$), whereas the Si and C atoms of the SiC matrix are evaporated under a high evaporation field.

The evaporation fields of the matrix and the nanoparticles have been evaluated from the C, Si and Fe Kingham curves [25] [26]. In our samples, Fe and Si are mainly evaporated in the Fe^{2+} and Si^{2+} ions, as can be observed in the mass spectrum. We also obtain the two C^+ and C^{2+} ions for the C atom. These considerations allow evaluating the Fe evaporation field close to 30 V/nm and the evaporation field of the matrix (only considering the C^+ and C^{2+} ions amounts of the same order for the C atom) close to 40 V/nm. The Fe evaporation field determined from the Fe Kingham curve is consistent with the pure Fe evaporation field (33 V/nm). This is not surprising because the nanoparticles contain Fe-rich phases. The evaporation field of the SiC matrix atoms is higher than the one of the nanoparticles atoms. Thus, it can be assumed that the atoms of the SiC matrix are evaporated under a mean evaporation field E_{SiC} ~ 40 V/nm, which is much higher than the evaporation field of nanoparticles [27].

Corresponding authors: lindor.diallo@etu.uni-rouen.fr

The difference of evaporation fields between the matrix and the nanoparticles leads to an over-density of atoms inside the nanoparticles and a sub-density of atoms around the nanoparticles in the 3D reconstructions, a well-known artifact of the APT.

The ratio between the evaporation fields of the particles and the matrix is close to 0.75. This ratio is very important to better understand the local magnification effects and trajectory overlaps leading to the 3D reconstruction process of the samples. It has been shown that for ratios smaller than ~0.6, the trajectories of the evaporated atoms lead to a negative magnification and a mixing of the atoms contained in the particles [26]. This was not the case for our samples with a f ratio (0.75) higher than 0.6. It means that only the first atomic shells are impacted by this phenomenon and are intermixed with the neighborhood of the matrix. Only the smallest particles (with a diameter smaller than ~2 nm) can be considered by this artifact rather than the biggest particles (up to 3 or 4 nm diameter).

Taking into account the true concentrations in the nanoparticles core, we know the number of Fe, Si and C atoms (N_{Fe}, N_{Si} and N_C, respectively) in the core and we can calculate the N_{Fe}/N_{Si} ratio. It appears that the values obtained for this ratio are very often close to 3.0, 2.0, 1.66 or 1, corresponding to the Fe_3Si, Fe_2Si, Fe_5Si_3 and FeSi core phases. This confirms that the APT artifacts do not impact the core of the biggest particles. We do not obtain a N_{Fe}/N_{Si} ratio higher than 3.0. Of course, all of these phases are not pure Fe-Si phases; they all contain a small amount of C atoms. In all the cases the C concentration is always smaller than the Si concentration. For the biggest nanoparticles (diameter ~7 to 12 nm) and the two Fe-richest phases, the C core concentrations are smaller than 10 at.%. The N_{Fe}/N_{Si} ratios are 3.00 ± 0.05 and 2.00 ± 0.05 and thus obtained with good accuracy. We do not find the Fe_8Si_2C or FeSiC phases or other ternary phases with a C concentration higher than the Si concentration [28]. Moreover, the Fe_3Si phase observed in the biggest nanoparticles of our samples has been characterized by Mössbauer spectrometry and exactly corresponds to the DO_3 structure [17]. Consequently, the C atoms enter the Fe_3Si phase, randomly and likely in interstitial sites rather than substitutional sites, but maintain the DO_3 structure of this phase.

We observed that the number of nanoparticles in a volume depends on the size. The biggest nanoparticles are the least numerous but also the Fe-richest (Fe_3Si and Fe_2Si phases). When the nanoparticles become smaller, they are more numerous but also less Fe-rich (Fe_5Si_3 and FeSi phases). When the nanoparticles become still smaller with a 2 or 3 nm order diameter, the core phase is hardly measurable due to the 1 nm order nanoparticle/matrix interface size and the APT artifacts described above.

Figure 3 represents Fe, Si and C atomic concentrations of the nanoparticles versus their average size. We can observe that, when the average size of the nanoparticles increases, the Si and C concentrations decreases and the Fe concentration increases. The C concentration decreases below 10 at.% for average size nanoparticles higher than 8 nm. For these nanoparticles, the Fe concentration is higher than 60 at.% allowing us to reach the Fe_3Si phase composition. We also observe that the Fe-richest nanoparticles (with Fe_3Si core phase) are obtained for the annealing performed at the highest temperature (here 1300°C). When the annealing temperature is lower than 1300°C (for example 1100 or 900°C but not shown here), we do not obtain the Fe_3Si phase. When the annealing temperature decreases, the core phases becomes less Fe-rich. This is perfectly consistent with the values of the enthalpy of formation of the Fe-Si phases that increase with the Fe amount contained in the Fe-Si phases and consequently with the annealing temperature [29].

Corresponding authors: lindor.diallo@etu.uni-rouen.fr

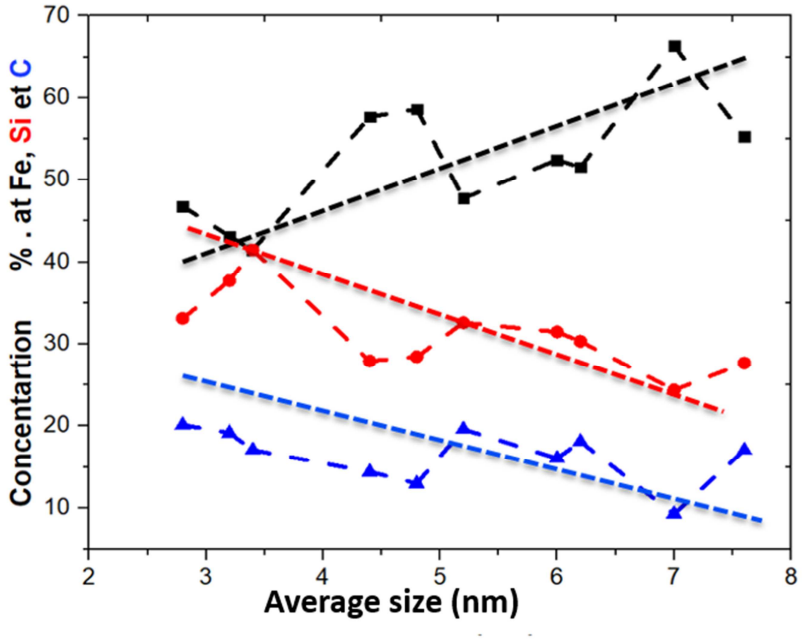

Fig. 3. Fe, Si and C atomic concentrations of the nanoparticles versus the average diameter size

Figure 4 shows a 3D reconstruction of a small volume containing only one nanoparticle (nanoparticle 3 taken as an example) and the corresponding concentration profile in the Z-direction of analysis. The cylinder used to determine the Si, C and Fe concentrations and plot the profile of Figure 4 (b) had a 0.5 nm diameter. Its size is sufficient to give an accurate profile of this nanoparticle. We can observe that the Fe, Si and C concentrations in the core of this nanoparticle are approximately 60, 30 and 10 at.% giving a N_{Fe}/N_{Si} ratio equal to 2. Thus, this nanoparticle contains a Fe_2Si type core phase with a small C amount (the C concentration being much lower than the Si one). Taking into account the C concentration (10 at.%), we are here in the presence of a non-pure Fe_2Si core phase as mentioned above, instead of a $Fe_{2(1-x)}Si_{(1-x)}C_{3x}$ type compound. According to these above observations, the present phase is the $Fe_{1.8}Si_{0.9}C_{0.3}$ phase which does not correspond to a Fe-Si-C stable ternary phase. Given that, all the nanoparticles are obtained in thin films samples and appear during 4 mn annealing and slow cooling processes. It is suitable to talk about Fe-Si phases with C amount rather than ternary Fe-Si-C phases because ternary particles predicted by ternary phase diagram were not observed. At the same time need to underline that the volume fraction of particles is not equilibrium one.

Corresponding authors: lindor.diallo@etu.uni-rouen.fr

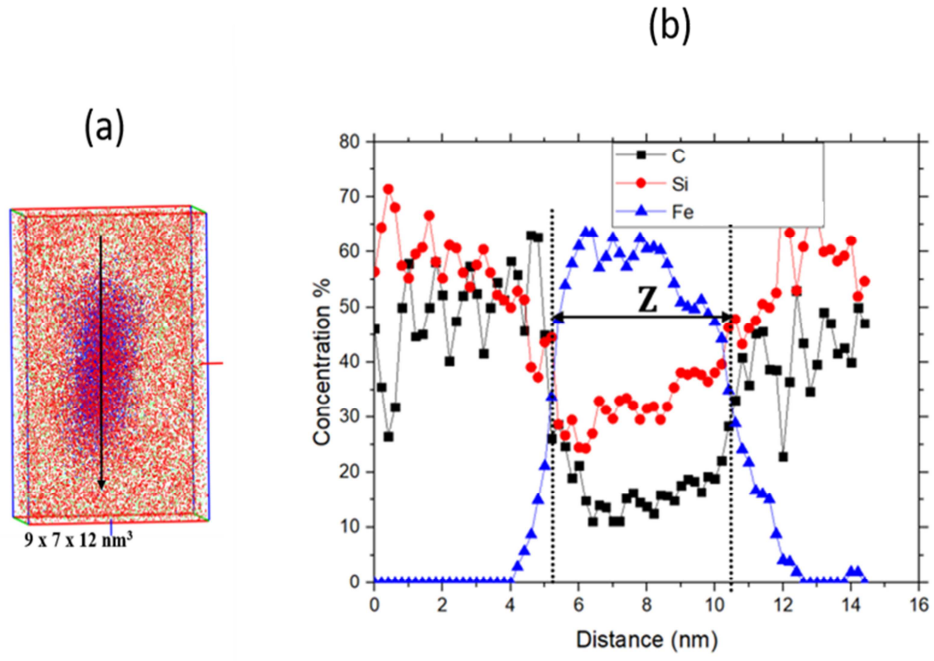

Figure 4: (a) 3D reconstruction of a small volume (9 x 7 x12 nm^3) containing only one nanoparticle and: (b) Corresponding Si, C and Fe concentration profile in the analysis Z-direction

3.3 As-implanted sample

Figure 5 shows 3D reconstructions of the same volume of the Fe as-implanted 6H-SiC sample; the Si, C and Fe atoms are represented in red, green and blue, respectively. We note that this sample has not been annealed, but has been maintained at 550°C for the entire duration of the Fe implantation. This sample does not contain Fe, Si and C nanoparticles as can be observed in these 3 reconstructions. This sample is perfectly diluted, semiconductor, but it is non–magnetic. It is the application of an annealing that can lead to the appearance of the magnetism. This annealing must be sufficient to generate magnetism without being so high that it minimizes the appearance of nanoparticles.

Corresponding authors: lindor.diallo@etu.uni-rouen.fr

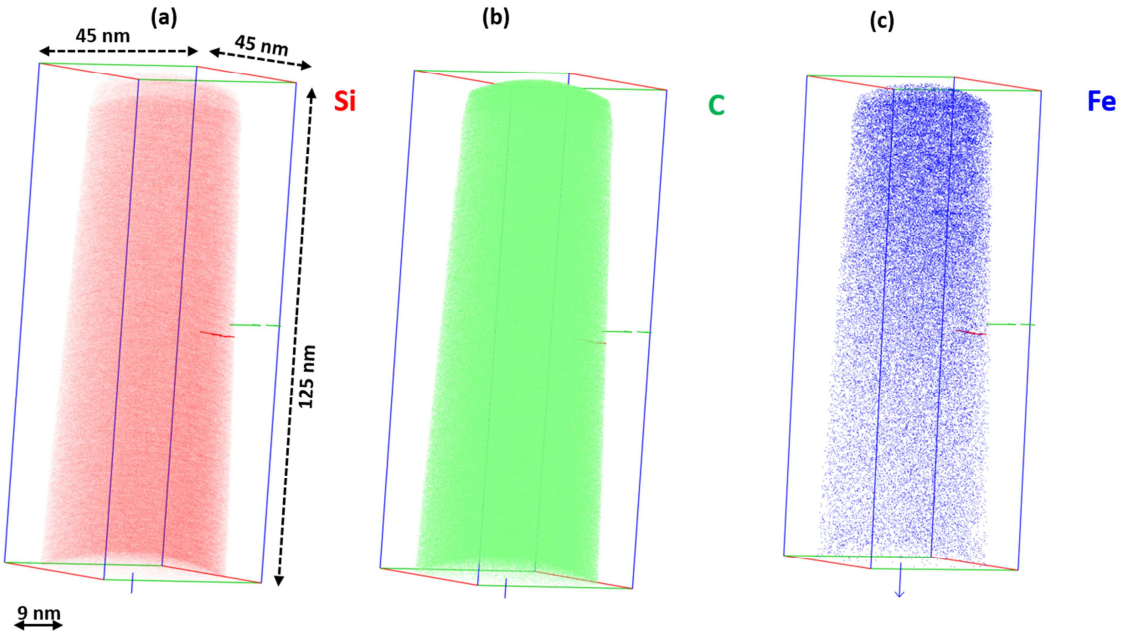

Figure 5: 3D reconstructions of the Si (a), C (b) and Fe (c) atoms of the 550°C Fe as-implanted sample

4. Conclusion

This work, performed by APT, shows that 550°C Fe-implanted 6H-SiC samples with a 2 at.% Fe concentration are perfectly diluted after implantation but contain nanoparticles after annealing. These particles mainly contain Fe-Si phases rather than Fe-C phases because of the great chemical affinity between the Fe and Si atoms. Thus, for the great majority of nanoparticles, the Si concentration is always higher than the C concentration. It is notably the case for the most annealed sample (1300°C) in which we can observe the Fe-richest (Fe-Si) phases, such as the Fe_3Si and Fe_2Si phases. Other less Fe-rich phases, such as the Fe_5Si_3 and FeSi phases, are also present in this sample, annealed only 4 minutes. All these phases are not pure (Fe-Si) phases but contain small C concentrations which are generally smaller than 10 at.% for the biggest nanoparticles. The annealing performed at lower temperatures (1100 and 900°C) also lead to the appearance of nanoparticles, but less Fe-rich. In the 1100 and 900°C annealed samples, we do not find the Fe_3Si and Fe_2Si phases. As mentioned above, the as-implanted sample is perfectly diluted but it is non-magnetic. It is the application of annealing (temperature, duration) that can lead to the formation of a magnetic sample but an annealing at too high a temperature also generates nanoparticles. To obtain a DMS with Fe-implanted 6H-SiC samples, it will be necessary to find an appropriate annealing (temperature and duration) and also perhaps an implantation temperature to generate magnetism in the samples to minimize the appearance of nanoparticles.

Acknowledgments

This work was funded by Region of Normandy and the European Regional Development Fund of Normandy (ERDF) in the frame of the MAGMA project. The authors would like to thank F. Danoix, F. Vurpillot, H. Zapolsky and D. Blavette for useful and fruitful discussions about APT.

Corresponding authors: lindor.diallo@etu.uni-rouen.fr

References

[1] H. Munekata, H. Ohno, S. Von Molnar, A. Segmuller, L. L. Chang, and L. Esaki, Phys. Rev. Lett. **63**, (1989) 1849.
[2] H. Ohno, A. Chen, F. Matsukara, A. Oiwa, A. Endo, S. Katsumoto, and Y. Iye , Appl. Phys. Lett., **69**, (1996) 363.
[3] T. Dietl, H. Ohno, and F. Matsukura, Phys. Rev. B **63**, (2001) 195205.
[4] A. Bonanni, and T. Dietl, Chem. Soc. Rev. 39, (2010) 528.
[5] A. V. Los, A. N. Timoshevskii, V. E. Los, S. A. Kalkuta, Phys. Rev. B, **76**, (2007) 165204.
[6] G. Bouzerar, and R. Bouzerar, C. R. Phys. **16**, (2015) 731.
[7] N. Theodoropoulou, A. F. Hebard, S. N. G. Chu, M. E. Overberg, C. R. Abernathy, S. J. Pearton, R. G. Wilson, J. M. Zavada, Sol. Stat. Lett. **12**, (2001) G119-121.
[8] F. Stromberg, W. Keune, X. Chen, S. Bedanta, H. Reuther and A. Mücklich. J. Phys.: Cond. Mat. **18** 43, 9881 (2006).
[9] C. Dupeyrat, Thesis University of Poitiers (2009).
[10] M. L. Diallo, L. Lechevallier, A. Fnidiki, R. Lardé, A. Debelle, L. Thomé, M. Viret, M. Marteau, D. Eyidi, A. Declémy, F. Cuvilly, and I. Blum, J. App. Phys. **117**, (2015) 183907.
[11] B. Song, J. K. Jian, H. Li, M. Lei, H. Q. Bao, X. L. Chen, G. Wang, Phys. Rev B, (2008) **403** 2897.
[12] B. Song, H. Bao, H. Li, M. Lei, J. Jian, J. Han, X. Zhang, S. Meng, W. Wang, and X. Chen, App. Phys. Lett **94**, (2009) 102508.
[13] Y. Liu, G. Wang, S. C. Wang, J. H. Yang, L. A. Chen, X. B. Qin, B. Song, B. Y. Wang, X. L. Chen, Phys. Rev. Lett **106,** (2011) 087205.
[14] V. A. Gubanov, C. Boekema C and C. Y. Fong, Appl. Phys. Lett. **78,** (2001) 216.
[15] Y. S. Kim, Y. C. Chung, and S. C. Yi, Mat. Sc. Eng. B **126**, (2006) 194.
[16] A. V. Los, A. N. Timoshevskii, V. F. Los, and S. Kalkuta, Phys. Rev. B **76**, (2007) 165 204.
[17] M. L. Diallo, L. Diallo, A. Fnidiki, L. Lechevallier, F. Cuvilly, I. Blum, M. Viret, M. Marteau, D. Eyidi, J. Juraszek, and A. Declémy, J. App. Phys **122**, (2017) 083905.
[18] L. Diallo , A. Fnidiki, L. Lechevallier, A. Zarefy, J. Juraszek, F. Cuvilly, I. Blum, M. Viret, M. Marteau, D. Eyidi, and A. Declémy, IEEE Mag. Let., **09,** (2018) 3103203.
[19] C. Dupeyrat, A. Declémy, M .Drouet, D. Eyidi, L. Thomé, A. Debelle, M. Viret, F. Ott, Physica B, **404**, (2009) 4731.
[20] A. Declémy, A. Debelle, C. Dupeyrat, L. Thomé, I. Monnet, and D. Eyidi, Appl. Phys. A **106,** (2012) 679.
[21] W. J. Weber, L. M. Wang, N. Yu, N. J. Hess, Mat. Sci. Eng. A, **62**, (1998) 253.
[22] K. Thompson, D. Lawrence, D. J. Larson, J. D. Olson, T. F. Kelly, and B. Gorman, Ultramicroscopy, **107**, (2007) 2-3, 131.
[23] M. H. Jonathan, G. Da Costa, C. Hatzoglou, H. Weekes, B. Radiguet, P. D. Styman, F. Vurpillot, C. Pareige, A. Etienne, G. Bonny, N. Castin, L. Malerba, and P. Pareige , Microsc. Microanal., 1-10, (2017).
[24] F. Zhang, and A. R. Oganov, Geophys. Res. Lett., **37**, (2010) 02305.
[25] D. R. Kingham, Sur. Sci., (1982)116 273.
[26] W. Lefebvre, F. Vurpillot, X. sauvage, Atom probe tomography, Put theory into practice, Elsevier (2016)
[27] R. Lardé, L. Lechevallier, A. Zarefy, A. Bostel, J. Juraszek, J. M. Le Breton, B. Rodmacq, and B. Dieny, J. App. Phys. **105**, (2009) 084307.
[28] S. J. Pearton, K. P. Lee, M. E. Overberg, C. R. Abernathy, N. Theodoropoulou, A. F. Hebard, R. G. Wilson and S. N. G. Chu, J. Elec. Mat. **31**, (2002) 16 .
[29] E.G. Moroni, W. Wolf, H. Hafner, and R. Podloucky, Phys. Rev. B, **59,** (1999) 860.

Corresponding authors: lindor.diallo@etu.uni-rouen.fr